Inoue et al., *Cogent Engineering* (2016), 3: 1231389
http://dx.doi.org/10.1080/23311916.2016.1231389

cogent engineering

BIOMEDICAL ENGINEERING | RESEARCH ARTICLE

Wind-tunnel experiment on aerodynamic characteristics of a runner using a moving-belt system

Tatsuya Inoue[1]*, Takafumi Okayama[1], Takahiro Teraoka[1], Satoshi Maeno[1] and Katsuya Hirata[1]

Received: 25 June 2016
Accepted: 28 August 2016
First Published: 07 September 2016

*Corresponding author: Tatsuya Inoue, Department of Mechanical Engineering, Doshisha University, Kyoto 610-0321, Japan
E-mail: euo1503@mail4.doshisha.ac.jp

Reviewing editor:
Zhongmin Jin, Xian Jiao Tong University China and Leeds University, UK

Additional information is available at the end of the article

Abstract: Wind-tunnel experiments are the most effective approaches both to elucidate the flows around runners in track-and-field athletics, and to evaluate their air resistances. In the present study, we develop a moving-belt system, and show its basic performance, such as the distributions of time-mean flow velocity and turbulent intensity above the moving-belt using a hot-wire anemometer. As a result, we have confirmed the effective improvement of the velocity distributions in terms of flow uniformity and turbulence reduction, especially near the moving-belt surface. Following, using this the developed moving-belt system, we investigate the air resistance on a runner in solo running and in duet running. For solo running, we reveal an increase in air resistance of more than 10% in comparison with the conventional result with no moving-belt system. For duet running, we reveal the optimum duet-running formation where a following runner behind a pacemaker experiences small air resistances or strong drafts.

Subjects: Aerospace Engineering; Biomechanics; Biophysics; Dynamics & Kinematics; Fluid Mechanics; Transport & Vehicle Engineering

Keywords: wind-tunnel; moving belt; ground effect; track runner; air resistance

ABOUT THE AUTHOR

Tatsuya Inoue is a researcher of fluid dynamics, affiliated to the Department of Mechanical Engineering, Doshisha University, Kyoto, Japan. My recent research interests include ground effect. Using this developed moving-belt system, we precisely evaluate the aerodynamic characteristics of models which move near the ground.

PUBLIC INTEREST STATEMENT

Wind tunnel experiments have been one of the most effective approaches to investigate aerodynamics. Moreover, moving-belt system is an important system, because that system can reproduce the real flow environment in wind-tunnel experiments. So, we develop a moving-belt system and confirm its basic performance. As the result, we get the good agreement between flow velocity distribution in wind-tunnel and it in real environment. Using this developed moving-belt system, we precisely evaluate the aerodynamic characteristics of models which move near the ground. This research, we use the runner models and precisely evaluate the drag of runners. For solo running, we revealed an increase in air resistance of more than 10% in comparison with the no moving belt results. For duet running, we revealed the place that the air resistance of the second runner decreases the most.

1. Introduction

Aerodynamics often becomes a crucial factor in various aspects of sports. Concerning most track-and-field athletics and marathons, it is important to elucidate the flow around runners, and to evaluate their air resistances or wind resistances. As air resistance is usually referred to as "drag" in aerodynamics, we hereinafter use the word drag in place of air resistance.

We are able to find similar studies dating as far back as the 1920s. Bois-Reymond (1925) and Hill (1927) conducted wind-tunnel experiments and reported the fluid forces acting on human models at various wind speeds. Their experimental results mostly agree with each other. After both pioneering works, several wind-tunnel experiments for the drag have been conducted (Belloli, Giappino, Robustelli, & Somaschini, 2016; Davis, 1980; Defraeye, Blocken, Koninckx, Hespel, & Carmeliet, 2010; Hoerner, 1958; Kawamura, 1953; Kyle, 1979; Martin, Milliken, Cobb, McFadden, & Coggan, 1998; Pugh, 1971, 1974; Raine, 1970; Shanebrook & Jaszczak, 1976; Spence, Thurman, Maher, & Wilson, 2012; van Ingen Schenau, 1982), although some of them are for skiing, cycling, horce-riding or skating instead of running to be exact. Recently, concerning the influence of the preceding runner upon the following runner, Ito (2006) carried out wind-tunnel experiments in addition to numerical analyses. According to Hill (1927), the drag of a runner is related to (1) air density, (2) the runner's projected area and (3) the square of his or her running speed, and accounts for 2–5% of his or her total resistance, which his muscles have to overcome. While Pugh (1970) did not conduct any wind-tunnel experiments, he showed the relation between the oxygen intake and the drag. According to Pugh, the contribution of the drag is large, that is, the energy cost of overcoming drag is estimated to be about 8% of the total energy cost for a 5,000-meter race and about 16% for a 100-meter sprint. Afterwards, Pugh (1971) further investigated the drag on a runner/walker, focusing on oxygen intake. Moreover, he discussed the influence of the preceding runner (pacemaker) upon the following runner in duet running, which is known as the drafting effect.

Wind-tunnel experiments have been one of the most effective approaches to such aerodynamic investigations, as well as numerical analyses, field measurements and so on. In wind-tunnel experiments, the moving-belt system is indispensable for precise aerodynamic measurements, if the concerning flow is affected by relation with the "ground effect." The ground effect means the influence that the ground gives to a model moving near the ground. When the model moves near the surface, it is thought that the ground relatively moves. In other words, the mean velocity distribution is different in the model is staying and it's moving. When model is moving, the flow velocity near the ground is accelerate. Moving belt system can accelerate velocity near the ground. Then, using this developed moving-belt system, we precisely evaluate the aerodynamic characteristics of models which move near the ground. In short, the ground effect for moving models just on stationary ground has been an interesting topic in fluid mechanics from both theoretical and practical points of view, relating to the existence/lack of a boundary layer on the ground.

Therefore, the ground effect must be accounted for, when we precisely investigate the aerodynamic characteristics of the prototypes or their scaled models in wind tunnels of (i) land vehicles such as trains, trucks, cars and (ii) taking-off/landing airplanes and creatures such as flying fishes (Davenport, 1992, 1994; Kawachi, Inada, & Azuma, 1993), as well as runners. Then the moving-belt system has progressively become important for accurate experiments of the ground effect in wind tunnels, which has been developed in various engineering aspects such as aeronautics (Hirooka & Takahashi, 1971; Nonaka, Kayaba, & Hayashi, 1998), road transportation (Berta, 1990; Lajos, Preszler, & Finta, 1986; Yoshida, Imaizumi, & Muto, 1985), railway transportation (Kikuchi, Nakagawa, Imao, & Kozato, 2011) and bluff-body aerodynamics (Yagita, Arimura, Kano, Inuzuka, & Tsukada, 1996). Unfortunately, for runners in track-and-field athletics and marathons, there have been no accurate wind-tunnel measurements using the moving-belt system, where we ignore the ground effect. In other words, all the previous wind-tunnel measurements were conducted on a stationary ground plate, where real running was not adequately reproduced.

In the present study, we attempt to develop a moving-belt system for accurate wind-tunnel experiments, and show its basic performance such as the profiles of time-mean flow velocity and turbulence intensity above the moving belt of the system using a hot-wire anemometer. Furthermore, we measure the vertical displacements of the moving belt by a laser displacement gauge. Then using this developed moving-belt system, we precisely evaluate the aerodynamic characteristics of a runner. First we reveal the drag of a runner in solo running. Second we investigate the drag of a runner in duet running with various duet-running formations to understand the aerodynamically effective formation for strong drafting.

2. Experimental method

2.1. Wind tunnel and moving-belt system

Figure 1(a) shows a schematic diagram of the present moving-belt system. We use a closed-return type (Gottingen-type) low-speed wind tunnel at Doshisha University. The wind tunnel has a closed test section (No. 1 in the Figure 1(a)) with a square cross section of 1,000 × 1,000 mm. The range of the mean velocity U_∞ of the mainstream is 5.0–30 m/s. Most of the present experiments are conducted at U_∞ = 5 and 10 m/s, where turbulence intensity is less than 0.2 and 0.5%, respectively. The corresponding values of the Reynolds number *Re* based on the present runner-model height, are 1.0×10^5 and 2.0×10^5, respectively. On the other hand, *Re* for actual runners varies from 5.0×10^5 to 2.0×10^6, which is much larger than the values of *Re* in the present wind-tunnel tests. This is not inconsistent, as we could usually ignore the influences of *Re* at $Re \gtrsim 10^3$, where flow is usually fully and turbulent being independent of *Re* (Wieselsberger, 1921).

The moving-belt system consists of a back plate (No. 8), an AC driving motor (No. 2), a coupling (No. 3), a driving roller (No. 5), a following roller (No. 9), a tension roller (No. 6), pulleys, V-belts (No. 4) and a front ground plate (No. 10) with the grating for boundary-layer suction control (hereinafter, referred to as BLSC), together with a moving belt (No. 7) with a thickness of 3 mm. The BLSC consists of a chamber (No. 11) and a cross-flow fan (No. 12), which is placed beneath the grating of the front ground plate.

Figure 1. Moving-belt system.

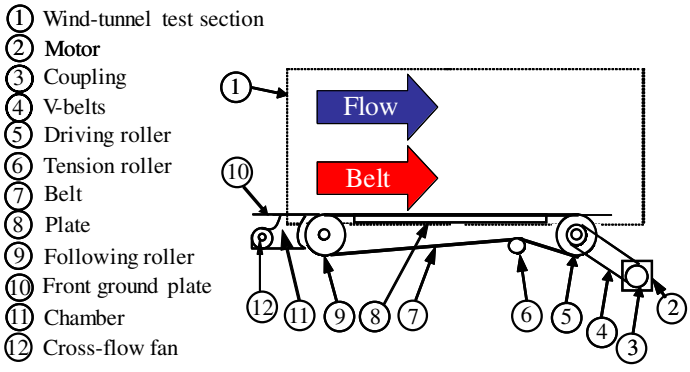

(a) Schematic diagram

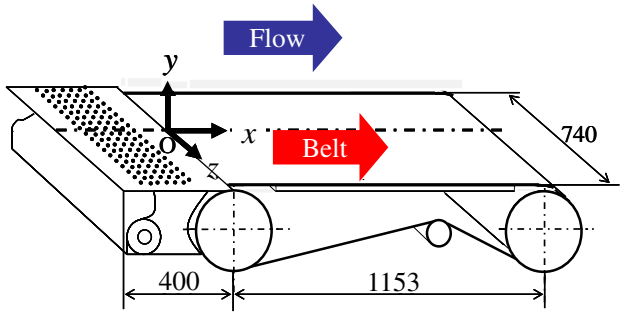

(b) Dimensions, together with a coordinate system (unit: mm)

Figure 1(b) shows the main dimensions of the moving-belt system, together with the present coordinate system. The origin O is at the center of the downstream end of the front ground plate. Both the *x* and *z* axes are horizontal in the streamwise and cross-streamwise directions, respectively. The *y* axis is vertical.

2.2. Runner model

Figure 2 shows a photograph of a wind-tunnel test section with a runner model, which is hung on the moving-belt by a wing-shape-cross-section cylinder (100 mm in chord, 15 mm in thickness and 500 mm in span) attached to a load cell. Like this, all the models are hung by the wing-shaped cylinders with the minimum narrow gap (≦4 mm) between the model and the moving-belt surface. More specifically, the model's back is connected to the wing-shaped cylinder by a supporting rod. As the blockage ratio is 1.8–2.0%, there are no corrections.

In the present study, the model is stationary with non-moving legs and arms. Therefore, we consider that the result averaged over 3 typical running postures; namely, 1 with the right-leg-back and the left-leg-forward (as seen in Figure 2), 1 with the right leg forward and the left leg back, and a neutral 1 between the 2.

When we consider duet running, we introduce an auxiliary coordinate system. Figure 3 shows the preceding runner (pacemaker) and the following runner in a duet-running formation, together with the auxiliary coordinate system.

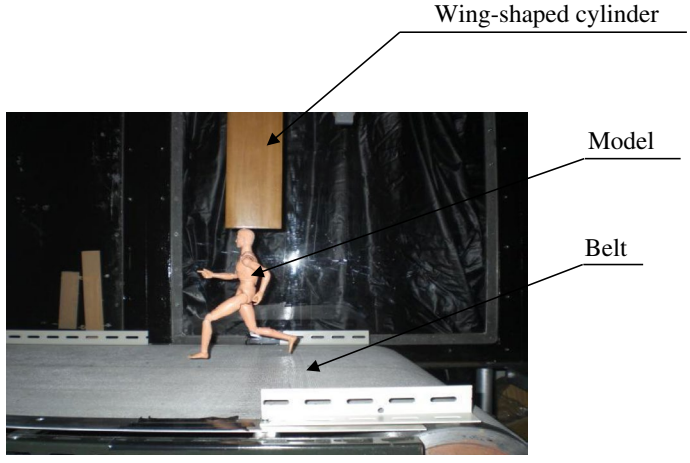

Figure 2. Photograph of a wind-tunnel test section with a runner model on the moving-belt system.

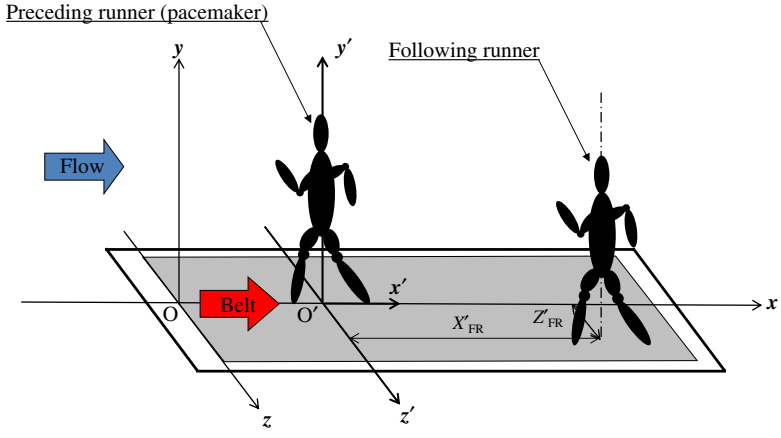

Figure 3. Preceding and following runners during duet running, together with the main and auxiliary coordinate systems.

3. Results and discussion

3.1. Basic performance of the moving-belt system

3.1.1. Moving-belt speed

First we specify the maximum value of the moving-belt speed V_b for precise measurement and long-term-stable operation. We have succeeded in raising V_b up to 13.0 m/s, over which the moving belt violently oscillates.

Second we check the accuracy of the DC/AC inverter to control the rotational speed of the AC driving motor. We suppose the theoretical moving-belt speed $V_{b,th}$, assuming the non-slips among the moving-belt, the driving roller, the pulleys, the V-belts and the AC driving motor. $V_{b,th}$ is predicted by a control parameter sent to the DC/AC inverter. The tested range of the actual moving-belt speed V_b, which is determined by high-speed-video-camera measurements, is 1.0–10 m/s. As the result, both V_b and $V_{b,th}$ are rigorously in proportion to n, while V_b is slightly smaller than $V_{b,th}$. Thus we can regard that the slip between the moving belt and the driving roller is negligible, as most of the measurements in solo and duet running are conducted at V_b = 5.0 m/s. From now on, we determine V_b from a modified $V_{b,th}$ using the calibration.

3.1.2. Oscillation of the moving-belt surface

Following this, we examine the moving-belt-surface oscillation in operation, at x = 0, 400, 600, 800 and 1,000 mm on the center line (at z = 0 mm). The tested value of V_b is fixed to 10 m/s, which is somewhat less than the maximum V_b (=13.0 m/s).

To confirm the amplitude of the moving-belt oscillation, the moving-belt-surface displacement y_b in the vertical direction is detected by a laser-displacement gauge fixed above the moving belt. As the result, y_b fluctuates in a range of 0.5–0.9 mm, due to the un-uniformity of the moving-belt surface, the vibration induced by the driving motor and so on. From now on, we conduct flow-velocity measurements by a hot-wire anemometer at $y \geq 4$ mm, considering the experimental reliability and the protection of a hot-wire-anemometer probe.

3.1.3. Mean-velocity profile

Afterward, we reveal mean-velocity profiles on the moving belt, at x = 200–1,000 mm on the center line (at z = 0 mm). Figure 4(a) shows an example of the profiles at x = 600 mm and U_∞ = 10 m/s. The abscissa represents the time-mean flow velocity $\bar{u}$ normalized by the mean velocity U_∞ of uniform mainstream. More specifically, $\bar{u}$ is obtained by means of averaging u over a long-enough period of about 120 s. In addition, the ordinate represents the vertical coordinate y normalized by the boundary-layer thickness δ, over which $\bar{u} > 0.99\, U_\infty$. We should notice that δ is estimated using experimental results shown in Figure 4(a). So, δ have varies values. In the Figure 4(a), open circles denote the results for the moving-belt system in operation; namely, the results on a moving belt with the BLSC. Both solid symbols denote the results for the moving-belt system out of operation; namely; more specifically, the solid squares and solid triangles for the results on a stationary belt with a BLSC and on a stationary belt without a BLSC, respectively.

First we compare the results obtained on the stationary belt with/without the BLSC. We do not confirm any clear effects of the BLSC upon the normalized mean-velocity profile, as the profile for the stationary belt with the BLSC almost coincides with that for the stationary belt without the BLSC. Both the profiles are close to the typical turbulent boundary layer with the logarithmic profile. Once more in Figure 5, we discuss the similarity to the turbulent boundary layer concerning the boundary-layer thickness.

Second if we compare the profile for the moving belt with both the profiles for the stationary belts, we can find a clear improvement. That is, we can achieve an almost flat profile by the moving-belt system. Strictly speaking, the value of $\bar{u}$ is less than U_∞ by about 5% at y = 4 mm, where the nearest

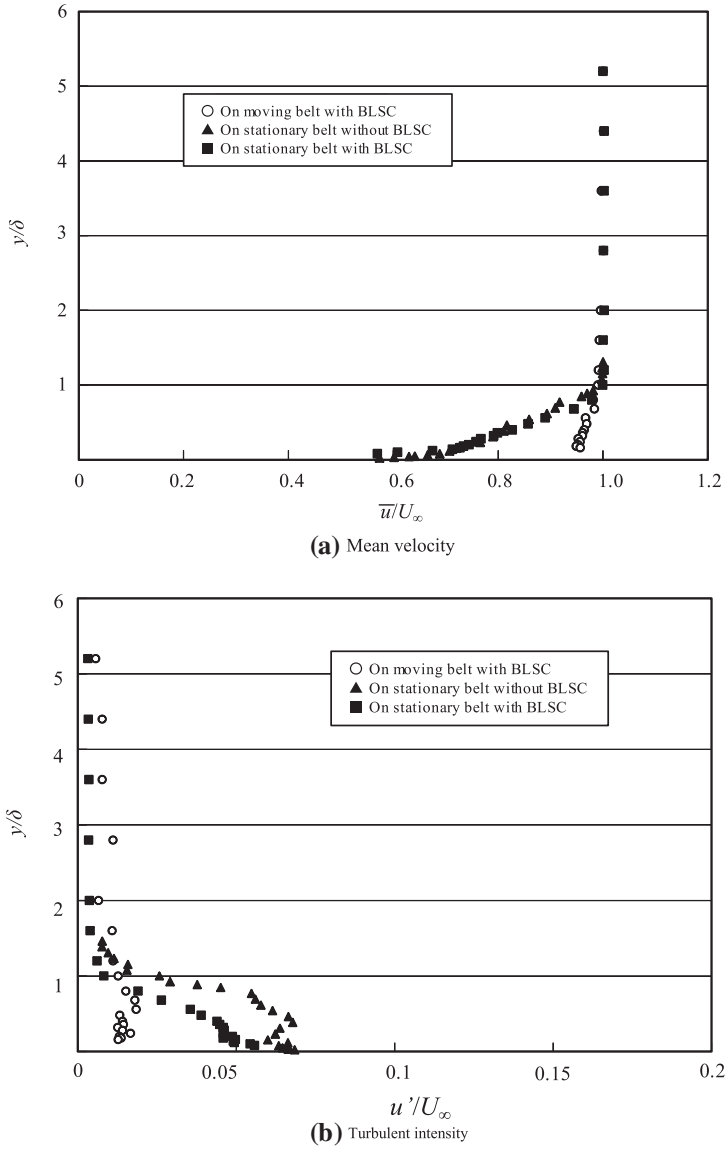

Figure 4. Velocity profiles (at x = 600 mm, z = 0 mm and U_∞ = 10.0 m/s).

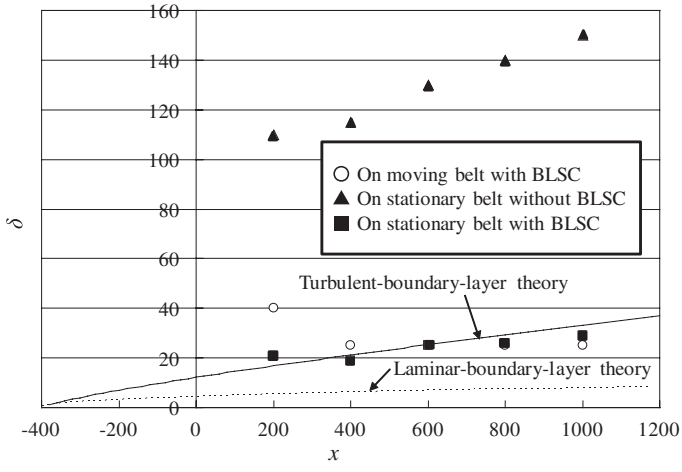

Figure 5. Distribution of boundary-layer thickness δ (at z = 0 mm and U_∞ = 10.0 m/s) (unit: mm).

measuring position to the moving-belt surface is. In order to avoid the risk of the oscillating moving belt breaking the hot-wire probe, we avoid any measurements at $y < 4$ mm, as mentioned above.

From mean-velocity profiles like those in Figure 4(a), we can specify boundary layer thickness δ, at each x on the center line (at $z = 0$ mm). Figure 5 shows the distribution of δ in the x-direction. The symbols in the Figure 5, namely, open circles, solid squares and solid triangles are the same as those defined in Figure 4(a). Solid and dotted lines denote the turbulent and laminar boundary layer theories (Morikawa, Ayukawa, & Tsuji, 1981), respectively. In both of these theories, we assume the virtual origin of the boundary layer exists at $x = -400$ mm, which corresponds to the upstream end of the leading ground plate.

First we compare the results on the stationary belt with/without the BLSC. We can see a clear effect of the BLSC upon the value of δ, in contrast with the mean-velocity profile as shown in Figure 4(a). Because of this, all values of δ without the BLSC are much larger than those with the BLSC and then the turbulent boundary layer theory. This is considered to be related to the surface roughness at the BLSC's grating, which could enhance turbulence inside the boundary layer.

Second we cannot see any clear effects of the moving-belt operation upon the value of δ, wherever the BLSC is activated. Again this is in contrast with the mean-velocity profile shown in Figure 4(a). This is because all the values of δ for both the operating and non-operating moving belt with the BLSC are close to 20 mm, which almost coincides with the turbulent boundary layer theory and is much larger than the laminar boundary layer theory. We can confirm the similarity to the turbulent boundary layer concerning the boundary-layer thickness. Therefore, the effect of the moving-belt operation itself is limited not only to the value of δ, but to the profiles near the moving belt surface. Incidentally, the discussion on δ for the operating moving belt is not strict, because its mean-velocity profile is much different from any typical boundary layers, as shown in Figure 4(a).

3.1.4. Turbulence-intensity profile

Finally, we reveal turbulence-intensity profiles on the moving belt, at $x = 200$–$1{,}000$ mm. Figure 4(b) shows an example of the profiles at $x = 600$ mm and $U_\infty = 10$ m/s. As well as in Figure 4(a), the abscissa represents the turbulence intensity normalized by U_∞. In addition, the ordinate represents the y normalized by δ. All the symbols are defined, as well as Figure 4(a) and Figure 5.

First we compare the results on the stationary belt with/without the BLSC. We can see that the effect of the BLSC upon the turbulence-intensity profile is slight but not negligible. $u'/U_\infty = 5.8\%$ with the BLSC and 7.0% without the BLSC at $y = 2$ mm. Then, the BLSC can achieve the improvement in turbulence-intensity reduction by 1.2%. Moreover, inside the boundary layer (at $y/\delta < 1$), u'/U_∞ for the former (the stationary belt with the BLSC) linearly decreases, as y/δ increases. On the other hand, u'/U_∞ for the latter (the stationary belt without the BLSC) keeps a high value of about 7%. Incidentally, outside the boundary layer (at $y/\delta > 1$), u'/U_∞ always equals about 0.2%, which is close to the original value of the present wind tunnel.

After that we compare to the moving belt with the BLSC to the stationary belt with the BLSC. By the moving-belt operation, we can find an obvious improvement, namely, we can achieve a reduction of about 1.2% of u'/U_∞ at $y/\delta = 0.16$ ($y = 4$ mm), and to 1.9% at $y/\delta \cong 0.6$. This is considered to be related to the improvement in the mean-velocity profile just near the surface of the operating moving belt, as shown in Figure 4(a). As a result, we can regard that the strength and direct influence of the moving belt operation is restricted at $y/\delta \leq 0.6$. Incidentally, outside the entire boundary layer (at $y/\delta > 1$), u'/U_∞ in the moving-belt operation is close to 1% which is much larger than 0.2%. This is considered to be related to the ambient-fluid vibrations together with the measuring-system structural vibrations and electrical noises induced by the driving motor. Of course, u'/U_∞ in the moving-belt operation at $y/\delta > 1$ is much smaller than that u'/U_∞ in the boundary layer at $y/\delta \leq 1$.

3.2. Aerodynamics in solo running

In this subsection, using the moving-belt system verified above, we evaluate the aerodynamic characteristics of a runner in solo running.

In general, the drag D acting on a runner is unsteady and fluctuates over time. Therefore, it is necessary to estimate the time-mean value of D, which is usually non-dimensionalised as drag coefficient C_D. We define C_D by $2D/\rho U_\infty{}^2 A$, where ρ denotes air density. We should note that A denotes the projected area of a runner in his or her running posture, according to the conventional usage in aerodynamics. On the other hand, depending on the running posture at each instant, this definition of A makes the estimation of the actual drag D difficult. From a practical point of view, A ought to be the projected area of a runner in his or her standing posture or the square of the height of a runner. Or we ought to suppose such a dimensional quantity as the drag area $C_D A$ instead of C_D, while the use of $C_D A$ is less general because of the dimensionality of $C_D A$.

Table 1 summarizes air resistance during solo running, namely, the drag coefficient C_{DSR} of a solo runner at $Re = 1.0 \times 10^5$ and $U_\infty = V_b = 5.0$ m/s together with other researcher's experiments. As the result, the present study on the moving belt with BLSC reveals that $C_{DSR} = 1.57$. Specifically, we first conduct time averaging and specify C_{DSR} on three kinds of running postures; one with the right leg forward and the left leg back, one vice versa (with the right leg back and the left leg forward) and one neutral (with both legs together) between the two running postures. We next conduct ensemble average over the three running postures: to be strict, $C_{DSR} = 1.81$ on the right leg forward, $C_{DSR} = 1.71$ on

Table 1. Drag coefficient C_{DSR} of a runner during solo running (at $Re = 1.0 \times 10^5$), together with other researchers' experiments. Numerical value in brackets represents C_{DSR} based on the projected area in a standing posture instead of a running posture

Author	Posture	C_{DSR}
Present (on moving belt with BLSC)	Running	1.57
		[1.37]
Present (on stationary belt without BLSC)	Running	1.36
		[1.17]
Hill (1927)	Running	0.9
	Standing	0.98
Kawamura (1953)	Racing in cycling	0.80–0.971
	Upright in cycling	0.912–1.14
Hoerner (1958)	Standing	1.0–1.3 (clothed)
		0.9–1.2 (nude)
Raine (1970)	Upright in skiing	1.0
	French egg in skiing	0.7
Pugh (1971)	Running	0.8
	walking	0.7
Pugh (1974)	Racing in cycling	0.79
Shanebrook and Jaszczak (1976)	Running	About 1.1 (cited by Kyle, 1985)
Kyle (1979)	Racing in cycling	0.79–0.82
	Upright in cycling	0.95–1.14
Davis (1980)	Running ($U_\infty < 15$ m/s)	0.87
Martin et al. (1998)	Uplight in cycling	0.84–1.27
Defraeye et al. (2010)	Cycling	0.62–0.65
Spence et al. (2012)	Horce-riding	0.90–1.00
Belloli et al. (2016)	Cycling (leading cyclist)	0.83–0.90
	Cycling (trailing cyclist)	0.43–0.63

the right leg back and C_{DSR} = 1.37 on the natural. Although the values of the former two running postures should be identical, the discrepancy between the obtained results is about 5% owing to the lack of strict antisymmetry in the runner's orientation and so on. C_D in the latter running posture (neutral) is obviously smaller than that in the former. This is considered to be related with less two-dimensionality in wake structure of the latter than the former owing to less stretched limbs in the latter, while we cannot further explain the reason for this drag reduction in the present stage to be exact.

Table 1 summarizes C_{DSR} not only on the moving belt but also on the stationary belt (that is, the non-operating moving belt) in a conventional style as well. As the result, the present study on the stationary belt without BLSC reveals that C_{DSR} = 1.36: to be strict, C_{DSR} = 1.61 on the right leg forward, C_{DSR} = 1.50 on the right leg back and C_{DSR} = 1.17 on the natural. We can see about a 13% increase in drag compared to the result without the moving-belt system, concerning not only each running posture but also the averaged value of the three running postures. This suggests that the ground effect should be considered even for evaluating the aerodynamic characteristics of runners. As one explanation for such a large increase in drag, we can hypothesize a remarkable change in flow patterns on the ground surface by the moving-belt operation, as well as a change in the mean-velocity and turbulence intensity profiles without any runner models by the moving-belt operation. In fact, in term of the flow visualization by smoke in the leeward side of a runner's leg, we observe an accompanying stream with the ground surface on the moving belt in contrast with the upward stream along the leg on the stationary belt.

Next, we compare the present results with other studies, as Table 1 also summarizes other researchers' experiments, namely, the drag coefficient C_{DSR} of a runner during solo running together with those during standing, cycling, skiing, walking and skating. Of course, the drag coefficients are detected using wind tunnels without the moving-belt systems. We see that the present result is close to Hoerner (1958) and Shanebrook and Jaszczak (1976), while drag coefficients are widely scattered in a range between 0.8 and 1.3. The supposed reasons for this scattering are boundary-layer thickness on a stationary belt/plate, the posture of the runner model, the details of the runner model and so on. It is thus difficult to specify the drag coefficient from a quantitative point of view at the present stage. However, at the very least, a conservative estimation for a system with no moving-belt would still be modified by about 10%

3.3. Aerodynamics during duet running

Next we consider the drag during duet running in order to reveal the optimum duet-running formation, where a runner running behind another runner experiences amount of small air resistance (or a strong drafting).

Figure 6(a) shows the drag coefficient C_{DFR} on moving belt (hereinafter, referred to as MB) with BLSC and C_{DFR} on stationary belt (hereinafter, referred to as SB) without BLSC of a following runner in tandem duet running (at $Z'_{FR}/h = 0$) plotted against the reduced streamwise distance X'_{FR}/h of the following runner from the preceding runner (the origin of X'_{FR}) at $Re = 1.0 \times 10^5$ (U_∞ = 5.0 m/s). Tandem-duet running is a special type of duet running where the following runner is to the leeward side of the preceding runner. We can see that the C_{DFR} for tandem duet running is smaller than the C_{DSR} for solo running by 50% or more, on both the moving and the stationary belts. All of this is in addition to the 20–30% increase in drag compared to the conventional result without the moving belt system.

Figure 6(b) shows the C_{DFR} on moving MB with BLSC and C_{DFR} on SB without BLSC not for tandem duet running but for off-set duet running at $Z'_{FR}/h = 0.18$ plotted against X'_{FR}/h. There and in Figure 6(a), we can see that C_{DFR} is smaller than C_{DSR} by more than 20% on both the moving and stationary belts. Besides there is an increase of 10–20% in drag compared to the conventional result on the stationary belt.

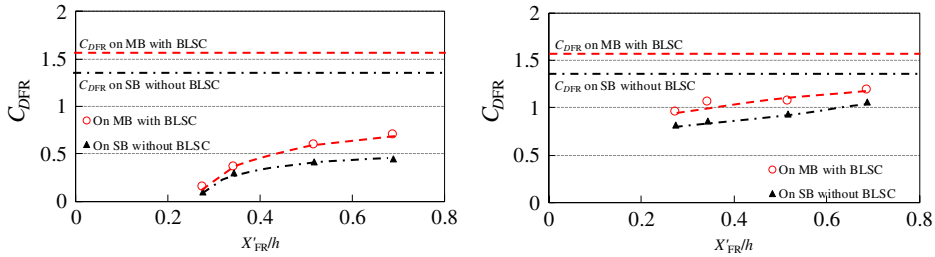

(a) During a tandem duet running (at $Z'_{FR}/h = 0$) **(b)** During off-set duet running (at $Z'_{FR}/h = 0.18$)

Figure 6. Drag coefficient C_{DFR} of a following runner against the reduced streamwise distance X'_{FR}/h of the following runner from a preceding runner (at $Re = 1.0 \times 10^5$).

Note: Each symbol represents the ensemble mean over measurements.

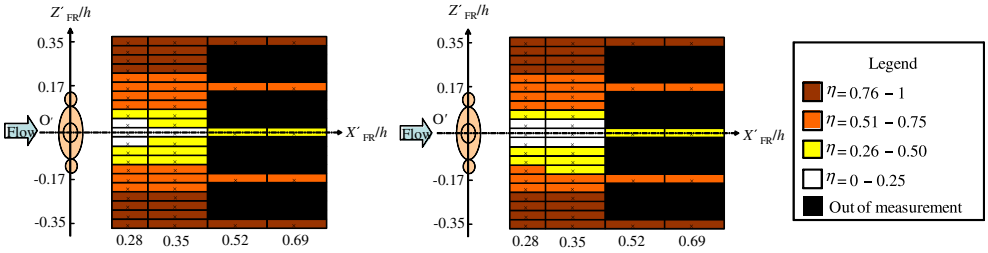

(a) On moving belt with BLSC **(b)** On stationary belt with BLSC

Figure 7. Distribution of drag ratio η behind a preceding runner during duet running compared to solo running (at $Re = 1.0 \times 10^5$).

Note: Crosses denote measuring positions.

Figure 7 summarizes all results related to duet running. Specifically, Figure 7 shows the distribution of drag ratio η ($\equiv C_{DFR}/C_{DSR}$) of a following runner behind a preceding runner in comparison with solo running at $Re = 1.0 \times 10^5$. Crosses in the Figure 7 denote measuring positions. Color represents the value of η as shown in the legend on the right hand side of the Figure 7. Figure 7(a) and (b) are the results for the operation with and without the moving-belt system, respectively. The effective formation shows that η ($=C_{DFR}/C_{DSR}$) is small case. For example, Figure 7(a) (on moving belt with BLSC) of the white color area ($\eta = 0$–0.25) is smaller than Figure 7 (b) (on stationary belt with BLSC). That is, we can see that the effective formation area on the moving belt with BLSC is smaller than it on the stationary belt with BLSC. In other words, the results with and without the moving-belt system are different from each other, when the runner is running near a preceding runner. Likewise, the results are the same, when the runner is running far from a preceding runner. From a quantitative point of view, an increase of 10–30% in drag can be observed compared to the conventional result without the moving-belt operation, (being independent of both X'_{FR}/h and Z'_{FR}/h). Finally, Pugh (1971) have shown the distribution of dynamic-pressure ratio ξ ($\equiv \bar{u}/U_\infty^2$) behind a preceding runner during solo running without the moving-belt system at $Re = 5.1 \times 10^5$. We should note that it seems difficult to find any similarities with the present results not only qualitatively but also quantitatively, as the experiment by him was conducted only several positions for solo running without the moving-belt system.

4. Conclusions

We have developed a moving-belt system, and have described features of its basic performance, such as the distributions of time-mean flow velocity and turbulent intensity above the moving-belt using a hot-wire anemometer. In addition, we have measured the vertical displacements of the moving belt through the use of a laser displacement gauge. As a result, we have successfully confirmed an effective improvement of the velocity distributions in terms of flow uniformity and turbulence reduction, especially near the moving-belt's surface. Using this moving-belt system, we have investigated the drag of a runner during solo running and during duet running. For solo running, we have revealed a more than 10% increase in air resistance compared to the conventional result with no moving-belt system. For duet running, we have revealed an effective duet-running formation where a following runner behind a preceding runner experiences a small drag. As a result, an aerodynamically-effective formation for smaller drag is thicker in comparison to the conventional wind-tunnel experiment with no moving-belt system.

Nomenclature

A	Projected area of a runner (mm^2)
C_D	Drag coefficient of a runner, $\equiv 2D/\rho U_\infty{}^2 A$
D	Drag of a runner (N)
h	Height of a runner; characteristic length scale (mm)
n	Inverter frequency (Hz)
Re	Reynolds number, $\equiv U_\infty h/\nu$
T	Period of one moving-belt revolution (s)
U_∞	Mean velocity of the uniform mainstream (m/s)
$\bar{u}$	Time-mean flow velocity (m/s)
u'	RMS of flow-velocity fluctuation (m/s)
V_b	Moving-belt velocity (m/s)
$V_{b,th}$	Theoretical V_b (m/s)
x, y, z	(Main) coordinate system (mm)
x', y', z'	Auxiliary coordinate system (mm)
y_b	Vertical displacement of the moving-belt surface (mm)
X'_{FR}	Streamwise distance from the preceding runner to the following runner (mm)
Z'_{FR}	Off-set (cross-streamwise) distance from the preceding runner to the following runner (mm)
δ	Boundary-layer thickness (mm)
η	Drag ratio, $\equiv C_{DFR}/C_{DSR}$
ξ	Dynamic-pressure ratio, $\equiv \bar{u}/U_\infty{}^2$
ν	Kinetic viscosity of air (m^2/s)
ρ	Density of air (kg/m^3)

Subscripts

BLSC	Boundary-layer suction control
FR	Following runner in duet running
MB	Moving belt
PR	Preceding runner (pacemaker) in duet running
SB	Stationary belt

SR Solo runner

Acknowledgements
We thank Mr Akiyoshi Oku (Carbon Magic Co., Ltd.) and Mr Nobuhiro Sasuga (Dome Co., Ltd.) for their valuable discussions and technical supports in experiments.

Funding
The authors received no direct funding for this research.

Author details
Tatsuya Inoue[1]
E-mail: euo1503@mail4.doshisha.ac.jp
Takafumi Okayama[1]
E-mail: duq0553@mail4.doshisha.ac.jp
Takahiro Teraoka[1]
E-mail: duq0573@mail4.doshisha.ac.jp
Satoshi Maeno[1]
E-mail: dup0578@mail4.doshisha.ac.jp
Katsuya Hirata[1]
E-mail: khirata@mail.doshisha.ac.jp
[1] Department of Mechanical Engineering, Doshisha University, Kyoto 610-0321, Japan.

Citation information
Cite this article as: Wind-tunnel experiment on aerodynamic characteristics of a runner using a moving-belt system, Tatsuya Inoue, Takafumi Okayama, Takahiro Teraoka, Satoshi Maeno & Katsuya Hirata, *Cogent Engineering* (2016), 3: 1231389.

References

Belloli, M., Giappino, S., Robustelli, F., & Somaschini, C. (2016). Drafting effect in cycling: Investigation by wind tunnel tests. *Procedia Engineering, 147*, 38–43. doi:10.1016/j.proeng.2016.06.186

Berta, C. (1990). Full-scale moving belt in Fiat aerodynamic wind tunnel. *SAE Paper, 905147*, 219–227.

Bois-Reymond, R. (1925). Der Luftwiderstand des menschlichen Körpers [The air resistance of the body]. *Pflügers Archiv für die Gesamte Physiologie des Menschen und der Tiere, 208*, 445–453.

Davenport, J. (1992). Wing-loading, stability and morphometric relationships in flying fish (Exocoetidae) from the North-eastern Atlantic. *Journal of the Marine Biological Association of the United Kingdom, 72*, 25–39. doi:10.1017/S0025315400048761

Davenport, J. (1994). How and why do flying fish fly? *Reviews in Fish Biology and Fisheries, 4*, 184–214. doi:10.1007/BF00044128

Davis, C. T. (1980). Effects of wind assistance and resistance on the forward motion of a runner. *Journal of Applied Physiology, 48*, 702–709.

Defraeye, T., Blocken, B., Koninckx, E., Hespel, P., & Carmeliet, J. (2010). Aerodynamic study of different cyclist positions: CFD analysis and full-scale wind-tunnel tests. *Journal of Biomechanics, 43*, 1262–1268. doi:10.1016/j.jbiomech.2010.01.025

Hill, A. V. (1927). The air-resistance to a runner. *Proceedings of the Royal Society of London Series B Biological Sciences, 102*, 380–385. doi:10.1098/rspb.1928.0012

Hirooka, K., & Takahashi, H. (1971). Moving-belt apparatus for low speed wind tunnel at NAL. *Journal of the Japan Society for Aeronautical and Space Sciences, 19*, 16–21. doi:10.2322/jjsass1969.19.94

Hoerner, S. F. (1958). *Fluid-dynamic drag* (pp. 3-14–3-15). Author.

Ito, S. (2006). Aerodynamic effects by marathon pacemakers on a main runner. *Transactions of the Japan Society of Mechanical Engineers Series B, 73*, 1975–1980. doi:10.1299/kikaib.73.1975

Kawachi, K., Inada, Y., & Azuma, A. (1993). Optimal flight path of flying fish. *Journal of Theoretical Biology, 163*, 145–159. doi:10.1006/jtbi.1993.1113

Kawamura, T. M. (1953). *Wind drag of bicycles* (Report No. 1). Tokyo: Tokyo University.

Kikuchi, S., Nakagawa, T., Imao, S., & Kozato, Y. (2011). The influence of airfoil profile and wing-tip plate on wing in ground effect. *Transactions of the Japan Society of Mechanical Engineers, 77*, 57–68. doi:10.1299/kikaib.77.2105

Kyle, C. R. (1979). Reduction of wind resistance and power output of racing cyclists and runners travelling in groups. *Ergonomics, 22*, 387–397. doi:10.1080/00140137908924623

Lajos, T., Preszler, L., & Finta, L. (1986). Effect of moving ground simulation on the flow past bus models. *Journal of Wind Engineering and Industrial Aerodynamics, 22*, 271–277. doi:10.1016/0167-6105(86)90090-5

Martin, J. C., Milliken, D. L., Cobb, J. E., McFadden, K. L., & Coggan, A. R. (1998). Validation of a mathematical model for road cycling power. *Journal of Applied Biomechanics, 14*, 276–291. http://dx.doi.org/10.1123/jab.14.3.276

Morikawa, Y., Ayukawa, K., & Tsuji, Y. (1981). *Nagaregaku* [Fluid dynamics] (pp. 80–85). Tokyo: AsakuraShoten.

Nonaka, O., Kayaba, S., & Hayashi, Y. (1998). Moving belt ground effect testing system of NAL 6.5 × 5.5 m low speed wind tunnel. *Technical Memorandum of National Aerospace Laboratory, 724*, 1–30.

Pugh, L. G. C. E. (1970). Oxygen intake in track and treadmill running with observations on the effect of air resistance. *The Journal of Physiology, 207*, 823–835. http://dx.doi.org/10.1113/jphysiol.1970.sp009097

Pugh, L. G. C. E. (1971). The influence of wind resistance in running and walking and the mechanical efficiency of work against horizontal or vertical forces. *The Journal of Physiology, 213*, 255–276. doi:10.1113/jphysiol.1971.sp009381

Pugh, L. G. C. E. (1974). The relation of oxygen intake and speed in competition cycling and comparative observations on the bicycle ergometer. *The Journal of Physiology, 241*, 795–808. doi:10.1113/jphysiol.1974.sp010685

Raine, A. E. (1970). The aerodynamics of skiing. *Journal of Science, 6*, 26–30.

Shanebrook, J. R., & Jaszczak, R. D. (1976). Aerodynamic drag analysis of runners. *Medicine and Science in Sports and Exercise, 8*, 43–45.

Spence, A. J., Thurman, A. S., Maher, M. J., & Wilson, A. M. (2012). Speed, pacing strategy and aerodynamic drafting in Thoroughbred horse racing. *Biology Letters, 8*, 678–681. doi:10.1098/rsbl.2011.1120

van Ingen Schenau, G. J. (1982). The influence of air friction in speed skating. *Journal of Biomechanics, 15*, 449–458. doi:10.1016/0021-9290(82)90081-1

Wieselsberger, C. (1921). Neuere Feststellungen Über die Gesetze des Flüssigkeits-und Luftwiderstands [New finding using the law about air resistance of the fluid]. *Physikalische Zeitschrift, 22*, 321–328.

Yagita, M., Arimura, K., Kano, I., Inuzuka, N., & Tsukada, T. (1996). Effects of a ground plate on magnus effect of a rotating cylinder. *Transactions of the Japan Society of Mechanical Engineers Series B, 62*, 1294–1299. http://dx.doi.org/10.1299/kikaib.62.1294

Yoshida, Y., Imaizumi, T., & Muto, M. (1985). Development of a moving-belt in the small-scale wind tunnel. *Transactions of Society of Automotive Engineers of Japan, 7*, 285–288.

Cogent Engineering **(ISSN: 2331-1916) is published by Cogent OA, part of Taylor & Francis Group.**